


RESEARCH

Open Access



aFGF gene-modified adipose-derived mesenchymal stem cells promote healing of full-thickness skin defects in diabetic rats

Yiren Zhu^{1†}, Pinhua Chen^{1,2,3,4,5†}, Zhengchao Zhang^{1,2,3,4,5}, XueYi He^{1,2,3,4,5}, Ruoli Wang^{1,2,3,4,5}, Qi Fang^{1,2,3,4,5}, Zhixian Xu^{1,2,3,4,5} and Wubing He^{1,2,3,4,5*} 

Abstract

Background Chronic diabetic wounds pose a significant clinical challenge due to the limited efficacy of current treatments. This study aimed to investigate the role and potential mechanisms of adipose-derived mesenchymal stem cells (ADSCs) overexpressing acidic fibroblast growth factor (aFGF) in diabetic wound healing in a rat model.

Methods ADSCs were genetically modified to achieve stable overexpression of aFGF. Varying doses of aFGF-ADSCs (1×10^6 , 2×10^6 , 3×10^6 , 4×10^6) were injected into the muscular tissue surrounding diabetic rat wounds. We assessed aFGF expression and its impact on various stages of wound healing, including angiogenesis, inflammatory response, epithelialization, and collagen deposition. Transcriptomic sequencing was performed to explore the underlying mechanisms driving enhanced wound healing.

Results Lentiviral transduction successfully induced stable aFGF overexpression in ADSCs. In vivo experiments revealed that varying doses of aFGF-ADSCs markedly enhanced wound healing in diabetic rats in a dose-dependent manner. The dose of 3×10^6 aFGF-ADSCs demonstrated the most significant effect. In the 3×10^6 aFGF-ADSCs group, expression levels of aFGF, CD31, and CD163 were significantly higher than in other groups ($p < 0.05$), while CD86 expression was significantly lower ($p < 0.05$).

Conclusion Single doses of aFGF-ADSCs comprehensively improved various aspects of wound repair in diabetic rats, offering a potential new approach for treating chronic diabetic wounds. The mechanism of action involves promoting angiogenesis, modulating inflammatory responses, accelerating epithelialization, and optimizing collagen deposition.

Keywords aFGF, ADSCs, Wound healing, Angiogenesis, Inflammatory modulation

[†]Yiren Zhu, and Pinhua Chen contributed equally to this work.

*Correspondence:

Wubing He

hewb120@sina.com

¹Shengli Clinical Medical College of Fujian Medical University, Fuzhou, Fujian 350001, China

²Department of Emergency Trauma Surgery, Fujian Provincial Hospital, Fuzhou, Fujian 350001, China

³Fuzhou University Affiliated Provincial Hospital, Fuzhou, Fujian 350001, China

⁴Fujian Trauma Medicine Center, Fuzhou, Fujian 350001, China

⁵Fujian Key Laboratory of Emergency Medicine, Fuzhou, Fujian 350001, China



© The Author(s) 2025. **Open Access** This article is licensed under a Creative Commons Attribution-NonCommercial-NoDerivatives 4.0 International License, which permits any non-commercial use, sharing, distribution and reproduction in any medium or format, as long as you give appropriate credit to the original author(s) and the source, provide a link to the Creative Commons licence, and indicate if you modified the licensed material. You do not have permission under this licence to share adapted material derived from this article or parts of it. The images or other third party material in this article are included in the article's Creative Commons licence, unless indicated otherwise in a credit line to the material. If material is not included in the article's Creative Commons licence and your intended use is not permitted by statutory regulation or exceeds the permitted use, you will need to obtain permission directly from the copyright holder. To view a copy of this licence, visit <http://creativecommons.org/licenses/by-nc-nd/4.0/>.

Introduction

The skin, as the largest organ in the human body, serves as a natural physical barrier against external stimuli [1]. Normal wound healing commences with blood coagulation and activation of inflammatory cells, followed by proliferation and migration of fibroblasts and keratinocytes, along with matrix deposition and angiogenesis [2]. Chronic wounds are defined as long-term injuries that fail to achieve complete anatomical and functional repair through normal healing processes after one month of clinical treatment [3, 4]. Various diseases or specific injuries can impede wound healing, notably diabetes, which disrupts the typically ordered and overlapping healing process. Common characteristics of chronic wounds include persistent bacterial biofilms, defective epithelial regeneration, reduced angiogenesis, and delayed extracellular matrix (ECM) remodeling [5, 6]. In the United States, annual medical expenditures related to wound care are estimated to range between \$31.7 billion and \$96.8 billion [7]. Traditional treatments for chronic, non-healing wounds include wound cleaning and dressing changes, local or systemic antibiotic application, various physical therapies, and skin grafting or flap transplantation when feasible. However, these treatments often yield unsatisfactory results due to the persistent and complex pathophysiological features of chronic wounds.

In recent years, many scholars domestically and internationally have proposed and applied new treatment concepts and methods for chronic, non-healing wounds. Particularly, numerous novel bioengineered artificial skin products have gained attention in wound repair. Research on bioengineered artificial skin primarily involves three aspects: seed cells, scaffold materials, and growth factors, which work synergistically to promote wound repair [8]. Seed cells provide a vital source for scaffold materials and can form cells with functional tissue properties [9]. Common stem cells in wound repair include epidermal stem cells, dermal stem cells, and mesenchymal stem cells. As a potential therapeutic approach to promote chronic wound regeneration and closure, stem cells possess self-renewal capabilities, multi-directional differentiation potential, and the ability to promote tissue repair and immune regulation [10–12]. Adipose-derived mesenchymal stem cells (ADSCs) are a type of multipotent stem cell found in adipose tissue with multi-directional differentiation capacity. Under different induction conditions, ADSCs can exhibit osteogenic, chondrogenic, and adipogenic abilities, and can even differentiate into cardiomyocytes, endothelial cells, and hematopoietic cells, among other lineages [13, 14]. Recent preclinical and clinical trials have greatly improved the application of ADSCs in treating severe burns and non-healing ulcers [15]. ADSCs can produce various growth factors, such as vascular endothelial growth factor (VEGF), hepatocyte

growth factor (HGF), and basic fibroblast growth factor (bFGF), which promote the restoration of wound blood supply and thereby improve graft survival rates [16]. ADSCs not only enhance fibroblast migration and proliferation but also inhibit collagen deposition and α -smooth muscle actin (α -SMA) expression in hypertrophic scar fibroblasts [17].

Acidic fibroblast growth factor (aFGF) is an autocrine or paracrine hormone. It is considered a mitogen due to its ability to broadly promote mitosis in various cell types and has garnered widespread attention for its roles in promoting angiogenesis, wound healing, and metabolic regulation [18–20]. aFGF was first identified in 1979 as an endothelial cell growth factor derived from bovine hypothalamus extracts [21]. Shortly thereafter, research revealed that heparin could bind to this growth factor and greatly enhance its mitogenic potential [22, 23].

Previous studies have shown that aFGF exerts concentration-dependent mitogenic and chemotactic effects on key cells involved in wound healing. For instance, the response of epidermal keratinocytes and vascular endothelial cells exhibits a typical “S”-shaped dose-response function, with no inhibitory effects at high concentrations. However, dermal fibroblasts show inhibitory effects at high aFGF concentrations, displaying a narrow, bell-shaped dose-response curve [24–26].

This concentration dependence also influences the application of aFGF in wound treatment. Blaber et al. demonstrated that topical application of 1.0 $\mu\text{g}/\text{cm}^2$ of aFGF combined with heparin showed significant therapeutic effects; however, doses of 0.1 $\mu\text{g}/\text{cm}^2$ or 10.0 $\mu\text{g}/\text{cm}^2$ did not show efficacy [27]. Hagerott et al. conducted a topical aFGF dose study using 0.6, 2.0, and 6.0 $\mu\text{g}/\text{cm}^2$, revealing that topical aFGF doses between 0.6 and 2.0 $\mu\text{g}/\text{cm}^2$ promoted wound healing, while the 6.0 $\mu\text{g}/\text{cm}^2$ dose significantly inhibited wound repair [28].

Both ADSCs and aFGF have demonstrated remarkable skin regeneration and vascularization capabilities in animal experiments and clinical applications. Hoseini et al. conducted an innovative study where they transfected ADSCs with aFGF in vitro and collected the culture supernatant to treat 3T3 cells and vascular endothelial cells (VECs) in vitro. The study revealed that, compared to the control group using regular culture medium, the experimental group's treatment significantly promoted the proliferation and migration of 3T3 cells and VECs, further enhancing the formation of new blood vessels [29]. However, in-depth research on the combination of aFGF and ADSCs for wound repair has not yet been conducted.

Based on these studies, we hypothesized that the combination of aFGF and ADSCs could promote wound repair, with the effect potentially exhibiting dose dependence. To test this hypothesis, we established a diabetic

rat wound model and evaluated the effects of different concentrations of aFGF-ADSCs (1×10^6 , 2×10^6 , 3×10^6 , 4×10^6) on wound healing.

The results showed that, compared to the negative control PBS and ADSCs alone, aFGF-ADSCs significantly promoted wound healing in diabetic rats. This effect was primarily achieved through the following mechanisms: promoting angiogenesis, suppressing inflammatory responses, and enhancing collagen deposition and remodeling (as shown in Fig. 1). Among these, 3×10^6 aFGF-ADSCs demonstrated the optimal promoting effect.

Our findings not only expand the understanding of the mechanisms by which ADSCs and aFGF promote wound healing but also offer a potential new approach for treating diabetic wounds.

Materials and methods

Isolation and culture of ADSCs

Three-week-old male Specific pathogen-free (SPF) Sprague-Dawley (SD) rats were purchased from Shanghai SLAC Laboratory Animal Co., Ltd. After one week of adaptive feeding, rat ADSCs were isolated from the inguinal adipose tissue of the rats and washed with phosphate-buffered saline (PBS; Gibco). The tissue was then minced and digested with 0.1% type I collagenase (BioFroxx) at 37 °C for 1 h. Enzyme activity was neutralized in DMEM/F12 (Gibco) containing 10% fetal bovine serum (FBS; Wisent, Thermo Scientific, USA). The neutralized cells were centrifuged at 1000 rpm for 5 min.

After centrifugation, the pellet was resuspended in DMEM/F12 containing 10% FBS. The isolated cells (2000 cells/cm²) were maintained in culture flasks and cultured in a 37 °C, 5% CO₂ incubator. Fresh culture medium was replaced every 2–3 days; cells were digested with trypsin (Gibco) for passaging when they reached 95% confluence, and were passaged to the second generation.

Confirmation of adipose-derived mesenchymal stem cell characteristics

Third-generation ADSCs were collected, washed with PBS, and incubated in the dark at 4 °C for 30 min with phycoerythrin (PE)-labeled anti-CD34, anti-CD45, anti-CD90, and anti-CD29 antibodies (eBioscience). Cells were stained with PE-labeled non-specific IgG and IgG1 κ (eBioscience) to assess background fluorescence. Cells were analyzed using a FACS Calibur flow cytometer (Becton Dickinson), and histograms were generated using FlowJo software V10.

For adipogenic and osteogenic differentiation, experiments were conducted according to the manufacturer's instructions (Cyagen). When third-generation ADSCs reached 80% confluence, the culture medium was replaced with adipogenic differentiation medium A for 3 days, then alternately replaced with medium B for 24 h. After approximately 21 days, cells were fixed with 50% ethanol for 5 min and stained with Oil Red O to confirm the formation of lipid droplets. When third-generation ADSCs reached 70% confluence, the culture medium was replaced with osteogenic reagent every 3 days. After

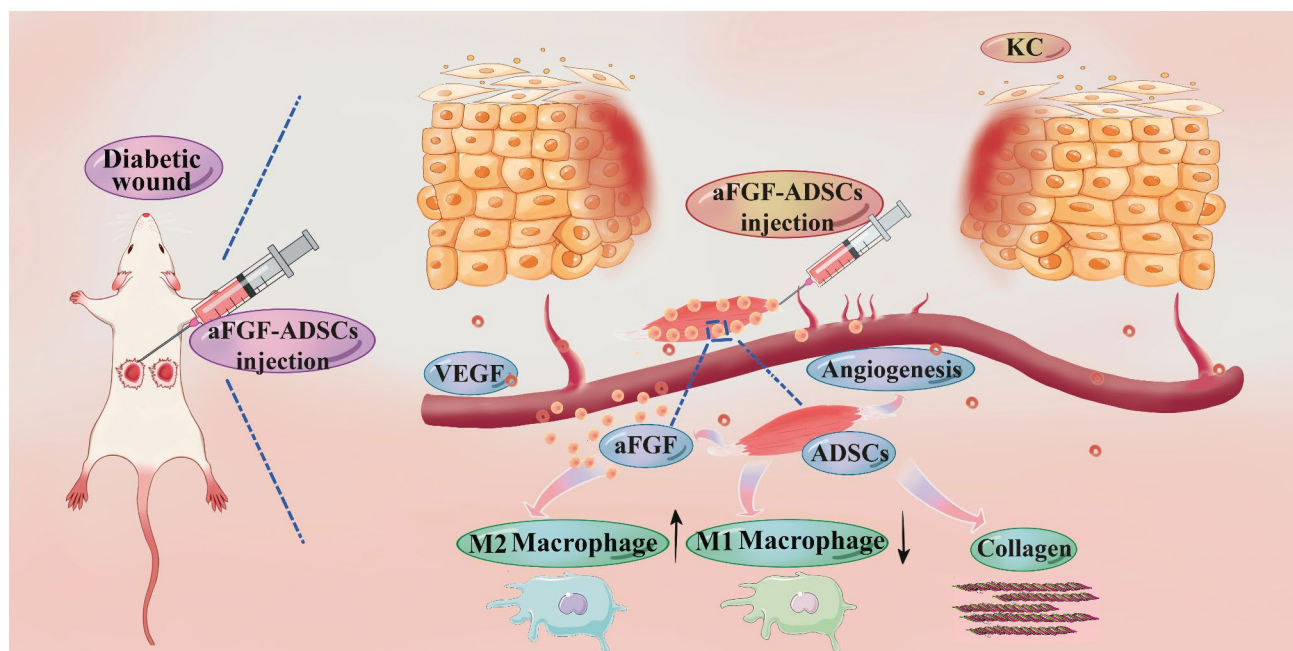


Fig. 1 aFGF gene-modified ADSCs promote wound healing in diabetic rats by enhancing angiogenesis, inhibiting inflammatory responses, and promoting collagen deposition and remodeling

21 days of culture, the presence of calcium nodules was evaluated by Alizarin Red staining. Finally, photographs of stained cells were taken using a microscope (Nikon, Japan).

Construction and identification of lentiviral vector carrying aFGF gene

The GV416-EF1a-MCS-3FLAG-aFGF-EGFP-T2A-PURO overexpression plasmid was purchased from Shanghai GeneChem Co., Ltd. To verify the aFGF overexpression plasmid, the synthesized overexpression plasmid was sent to Sangya Company for sequencing, and the sequencing results were compared with aFGF (NM_012846.2) using SnapGene.

Transfection was performed using Lipofectamine 3000 (Invitrogen, Thermo Scientific, USA) according to instructions. Viral supernatant produced by 293T cells through plasmid and Lipofectamine 3000 kit packaging was collected and mixed with ADSCs culture medium to obtain transfected cells.

Western blot

Total protein extraction was performed using RIPA buffer (Beyotime, Shanghai) supplemented with protease inhibitor cocktail (Beyotime, Shanghai). Protein concentration was measured using a bicinchoninic acid (BCA) protein assay kit (Beyotime, Shanghai) according to the manufacturer's instructions, and proteins were separated by sodium dodecyl sulfate-polyacrylamide gel electrophoresis (SDS-PAGE). Separated proteins were transferred to polyvinylidene difluoride (PVDF) membranes (Beyotime, Shanghai) and blocked with 5% skim milk (BD Difco, Thermo Scientific, USA).

Subsequently, PVDF membranes were incubated overnight at 4°C with rabbit polyclonal antibodies against aFGF (Abcam), GAPDH (Abcam), and mouse monoclonal antibody against Flag (Proteintech), followed by incubation with horseradish peroxidase-conjugated secondary antibodies (Abcam, Thermo Scientific, USA). Signal bands were detected using the Supersignal West Femto kit (Thermo Scientific, USA).

Quantitative real-time polymerase chain reaction (qRT-PCR)

Total cellular RNA was extracted using TRIzol (Invitrogen) and reverse transcribed using the PrimeScript® RT reagent kit (Takara) according to the manufacturer's instructions. The first-strand cDNA obtained from 800 ng of total RNA was used to measure aFGF expression and served as a template for quantitative real-time PCR, using the following primers: aFGF (F): AAGAAGCACG CGGAGAAGAA, (R): GCTTTCTGGCCGTAGTGAGT; 18 S (F): AGAAACGGCTACCACATCCA, (R): CACCA GACTTGCCCTCCA. Quantitative real-time PCR was

performed using corresponding primers and cDNA template, mixed with reagents from the SYBR Premix Ex Taq II kit (DRR081, Takara). Data were analyzed and quantified using the $\Delta\Delta C_t$ method, with the transcription level of each gene normalized to 18 S in the same sample.

Diabetic wound model and wound healing assessment

Forty-eight SPF male SD rats, 3 weeks old, weighing 60–80 g, were obtained from Shanghai SLAC Laboratory Animal Co., Ltd. and housed in the Animal Center of Mengchao Hepatobiliary Hospital of Fujian Medical University. The animals were maintained in individually ventilated cages (IVCs) under controlled environmental conditions, with a temperature of 25 ± 2 °C, humidity of $50 \pm 10\%$, and a 12-hour light/dark cycle, with ad libitum access to food and water. Following a 1-week acclimatization period, rats were fasted for 16 h and subsequently administered streptozotocin (45 mg/kg, Rhawn) via intraperitoneal injection for three consecutive days to induce diabetes. Random blood glucose levels were measured at the same time point weekly for 4 weeks. Rats exhibiting random blood glucose levels > 16.8 mmol/L and presenting classic diabetic symptoms, including polydipsia, polyphagia, and polyuria, were designated as diabetic and selected for the study. Rats with body weight loss exceeding 20%, random blood glucose levels ≤ 16.7 mmol/L, or those unable to survive were excluded. Ultimately, all 48 rats were successfully model-induced and included in the research.

Diabetic rats were anesthetized via intraperitoneal injection of 3% pentobarbital sodium (50 mg/kg). Back hair was removed, and two full-thickness circular wounds with a diameter of 10 mm were created on both sides of the dorsal midline. A 3 M silicone ring was sutured around the wound to prevent contraction. Using a random number table, rats were randomly allocated into 6 treatment groups ($n = 8$ per group, 16 wounds per group): Group A: PBS; Group B: 1×10^6 Vector-ADSCs; Group C: 1×10^6 aFGF-ADSCs; Group D: 2×10^6 aFGF-ADSCs; Group E: 3×10^6 aFGF-ADSCs; Group F: 4×10^6 aFGF-ADSCs. Each group was resuspended in 100 μ l PBS and injected into four quadrants of each wound. Wounds were covered with sterile Tegaderm dressings (3 M Healthcare), which were changed every other day until wound healing.

Digital photographs of the wounds were captured on postoperative days 0, 1, 3, 7, 10, 14, and 16. Wound size was quantified using ImageJ software. All animal experiments were ethically reviewed by the Institutional Animal Care and Use Committee (IACUC) of Fujian Provincial Hospital, with the ethical review number IACUC-FPH-SL-20240321. This study adhered to the ARRIVE guidelines 2.0 for reporting animal research. In strict adherence to the IACUC guidelines, animals were

humanely euthanized utilizing automated carbon dioxide (CO₂) displacement chambers, following the approved institutional protocol for rodent euthanasia. The experimental design is shown in Fig. 2.

Histological observation

Tissue samples collected on days 3, 7 and 16 post-wounding were fixed overnight in 4% paraformaldehyde at 4 °C. After fixation, samples were washed with PBS, dehydrated through a graded ethanol series (30%, 50%, 70%, 80%, 90%, and 100%), xylene, and paraffin, then embedded in paraffin. Sections 4–6 µm thick were prepared from paraffin-embedded wound tissues and subjected to hematoxylin-eosin (H&E) staining, Masson's trichrome staining, and Sirius red staining. Tissue sections were observed under a microscope.

Immunohistochemistry

Sections were prepared as described above. For immunohistochemistry, sections were deparaffinized in xylene and rehydrated through a graded ethanol series. Antigen retrieval was performed using citrate antigen retrieval solution under high pressure, followed by incubation with 3% hydrogen peroxide at room temperature for 20 min. Sections were incubated overnight at 4 °C with antibodies against aFGF, CD31, CD86, and CD163, then incubated with horseradish peroxidase-labeled secondary antibodies at 37 °C for 30 min. Subsequently, 3,3'-diaminobenzidine (DAB) was added for 10 min at room temperature, followed by hematoxylin staining for 2 min at room temperature. Finally, sections were gently washed with deionized water, dehydrated through graded ethanol solutions, mounted with neutral resin, and observed under an optical microscope.

Immunofluorescence

Anti-K10 and anti-K14 antibodies were used for immunofluorescence. Sections were incubated with the aforementioned primary antibodies overnight at 4 °C, followed by incubation with secondary antibodies at 37 °C for 1 h.

Finally, sections were stained with 4',6-diamidino-2-phenylindole (DAPI, Invitrogen, Carlsbad, CA) and observed under a Zeiss LSM 700 confocal fluorescence microscope (ZEISS, Germany).

Transcriptomics

Total RNA was extracted using Trizol reagent (Invitrogen) according to the manufacturer's protocol. RNA quality was assessed by Beijing Berry Genomics Corporation. After RNA samples passed quality control, standard transcriptome library construction was performed, followed by sequencing using Illumina NovaSeq 6000 after library quality control. Principal component analysis (PCA) was conducted using the R package gmodels. Differential expression analysis of RNA between two groups was performed using DESeq2 software. Gene Ontology (GO), Kyoto Encyclopedia of Genes and Genomes (KEGG), and correlation analyses were conducted to explore functions and signaling pathways associated with differentially expressed genes (DEGs). Data and visualization analyses were performed using Bioinformatics (www.bioinformatics.com.cn).

Data analysis

To minimize potential bias, blinding was implemented during data collection and analysis, with all procedures performed by personnel unaware of group allocations. This encompassed histological evaluations, fluorescence signal acquisition, and all analyses of tissue sections. Data analysis and graphing were conducted using SPSS 25.0 software (IBM, USA) and GraphPad Prism 9.0 software. Comparisons between two groups were performed using t-tests, while comparisons among multiple groups utilized one-way analysis of variance (ANOVA). Data were expressed as mean ± standard deviation (SD). Statistical significance was determined as follows: * $p < 0.05$; ** $p < 0.01$; *** $p < 0.001$; **** $p < 0.0001$; When $p > 0.05$, differences were considered not statistically significant (NS).

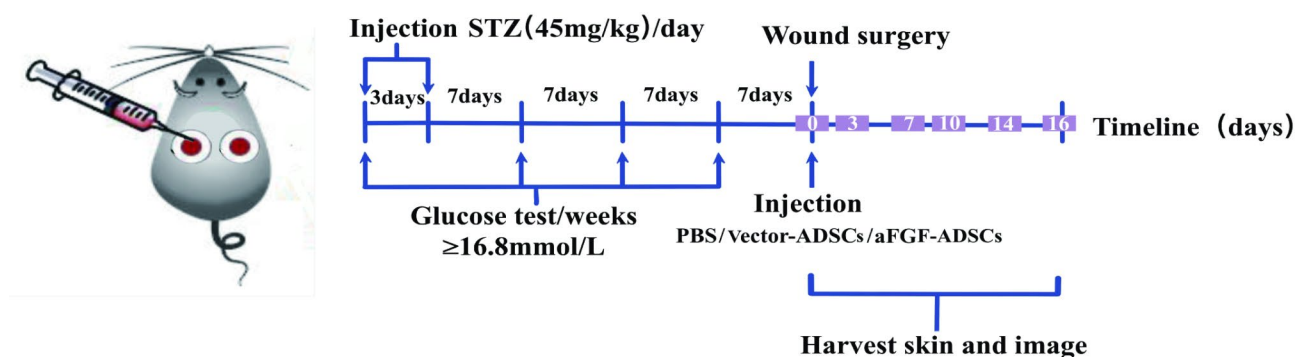


Fig. 2 Schematic illustration of diabetic rat model establishment and experimental timeline

Results

Characterization and identification of ADSCs

Rat inguinal adipose tissue was digested into a single-cell suspension using enzymatic digestion and cultured to P3 generation. Under an inverted microscope, ADSCs exhibited a spindle-shaped morphology (Fig. 3A). To verify the multi-lineage differentiation potential of P3 ADSCs, we conducted adipogenic and osteogenic induction experiments. After osteogenic induction, Alizarin Red staining distinct obvious calcium nodule formation (Fig. 3B). After adipogenic induction, Oil Red O staining showed clear lipid droplet formation (Fig. 3C). Finally, we measured the expression of two mesenchymal stem cell (MSC) surface antigens (CD29 and CD90) and two endothelial progenitor cell markers (CD34 and CD45) by flow

cytometry to confirm the MSC identity of the isolated ADSCs. Flow cytometry results showed positive expression of CD29 and CD90, while CD34 and CD45 expression was negative, confirming the MSC identity of the isolated ADSCs (Fig. 3D). In summary, this study successfully isolated ADSCs and confirmed their multi-lineage differentiation potential.

Construction and verification of aFGF-ADSCs

We first purchased the empty vector plasmid GV416-EF1a-MCS-EGFP-T2A-PURO and the over-expression plasmid GV416-EF1a-MCS-3FLAG-aFGF-EGFP-T2A-PURO (Genechem Company). The purchased recombinant plasmids were sequenced and compared with the aFGF (NM_012846.2) sequence

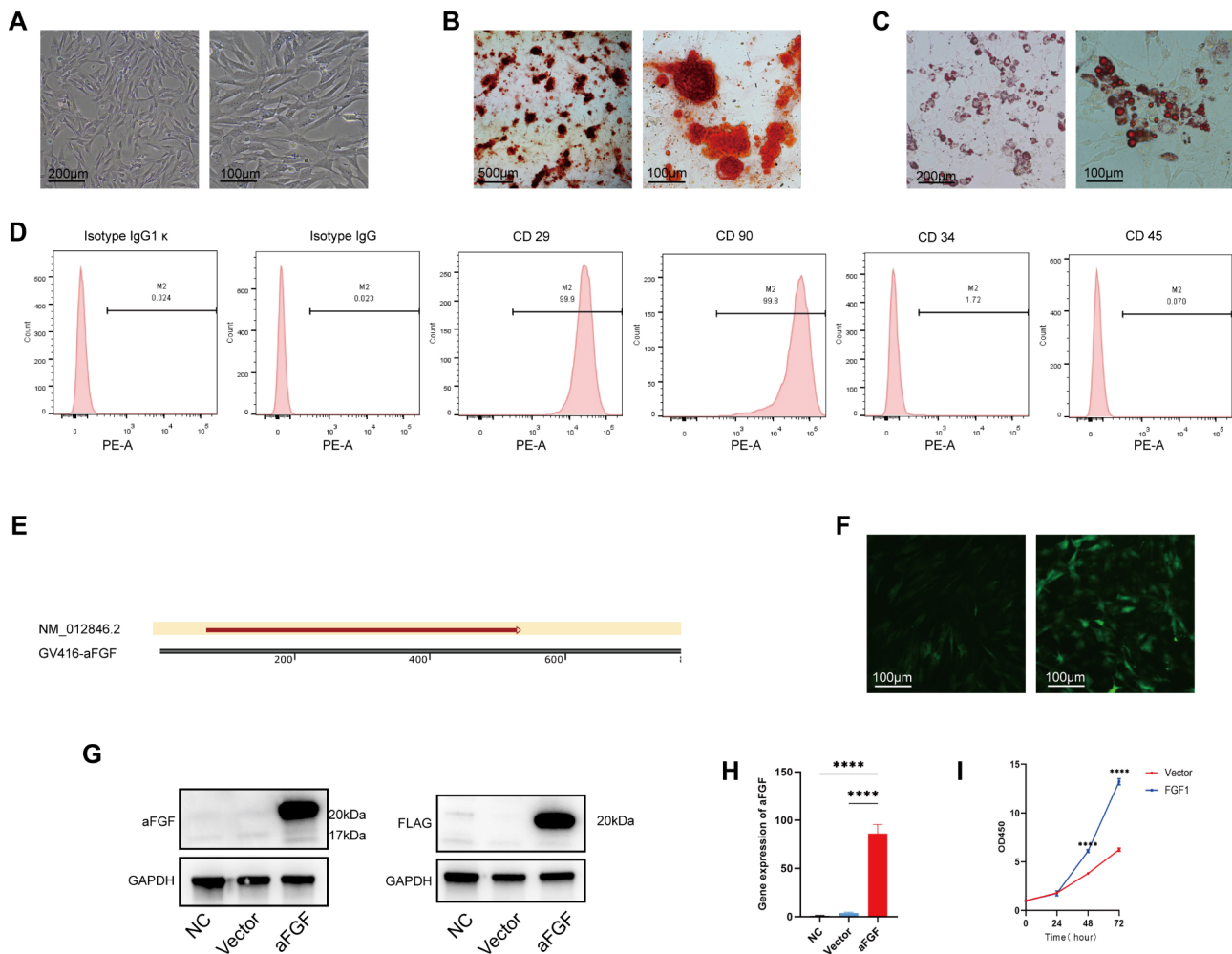


Fig. 3 Characterization of ADSCs and construction and identification of aFGF-ADSCs. **(A)** Isolated and cultured P3 ADSCs exhibit a flat spindle shape. **(B)** After osteogenic induction, bone nodules were detected by Alizarin Red staining. **(C)** After adipogenic induction, lipid droplets were detected by Oil Red O staining. **(D)** Immunophenotypic analysis of P3 ADSCs by flow cytometry showed positive expression of CD29 and CD90, and negative expression of CD34 and CD45, demonstrating typical MSC surface antigens. **(E)** Comparison of the overexpression plasmid using SnapGene. **(F)** Fluorescence microscopy of Vector-ADSCs (left) and aFGF-ADSCs (right). **(G)** Western blot analysis revealed significantly increased expression of Flag-aFGF in the aFGF-ADSCs group (Full-length gels are presented in Supplementary Fig. 1). **(H)** aFGF mRNA expression was significantly elevated in the aFGF-ADSCs group. **(I)** Cell proliferation activity assessed by CCK8 showed markedly enhanced proliferation of aFGF-ADSCs. ****: $p < 0.0001$

on NCBI, and no base pair mutations were found (Fig. 3E). Subsequently, we packaged lentivirus using 293T cells with empty vector and overexpression plasmids respectively, and then infected ADSCs with these viral supernatants to construct vector control ADSCs (Vector-ADSCs) and aFGF-overexpressing ADSCs (aFGF-ADSCs). After 72 h of culture, green fluorescence was observed under a fluorescence microscope in both Vector-ADSCs and aFGF-ADSCs, with significantly higher fluorescence intensity in aFGF-ADSCs compared to Vector-ADSCs (Fig. 3F). Next, we collected ADSCs, Vector-ADSCs, and aFGF-ADSCs, extracted RNA and protein for analysis. qRT-PCR and Western blot results confirmed that aFGF expression in aFGF-ADSCs was significantly increased at both transcriptional and protein levels compared to the control group (Fig. 3G and H). Finally, CCK-8 quantitative experiments showed that aFGF-ADSCs significantly enhanced cell proliferation activity after 48 hours (Fig. 3I). In conclusion, we successfully constructed aFGF-ADSCs that stably overexpress aFGF and significantly promote cell proliferation.

Different concentrations of aFGF-ADSCs promote diabetic wound healing

A diabetic rat model was induced by intraperitoneal injection of streptozotocin (STZ). Rats with random blood glucose levels >16.8 mmol/L for three consecutive measurements were selected, and two full-thickness skin wounds, each approximately 1 cm in diameter, were created on their backs. Forty-eight successfully modeled diabetic rats were randomly divided into 6 groups and injected with PBS (control group), 1×10^6 Vector-ADSCs, 1×10^6 , 2×10^6 , 3×10^6 , and 4×10^6 aFGF-ADSCs, respectively. The skin wound area was examined and photographed every 2–3 days. The results showed that compared with the PBS control group and Vector-ADSCs group, all doses of aFGF-ADSCs groups significantly promoted wound healing, with the 3×10^6 aFGF-ADSCs group achieving the highest closure rate (Fig. 4A and B). Immunohistochemical analysis of wound tissue on day 3 showed that aFGF content in the tissue surrounding the wound was significantly increased in all aFGF-ADSCs groups. The aFGF content was positively correlated with the number of injected cells, with the 3×10^6 and 4×10^6 aFGF-ADSCs groups exhibiting the highest levels (Fig. 4C and D). H&E and Masson staining were used to evaluate epithelial and collagen deposition on day 16 post-wounding. The results showed that the epithelium in all aFGF-ADSCs groups was more mature than the control group, with reduced inflammatory response and denser collagen deposition (Fig. 4E and F).

aFGF-ADSCs promote wound repair by enhancing angiogenesis, regulating inflammatory response, and promoting epithelial and collagen maturation

We assessed early wound neovascularization by immunohistochemical detection of the vascular marker CD31. The results showed that Vector-ADSCs and all aFGF-ADSCs groups promoted increased CD31 expression, with the 3×10^6 aFGF-ADSCs group exhibiting the strongest expression and the highest number of new blood vessels (Fig. 5A and F). The inflammatory response in each group was compared by detecting the M1 macrophage surface marker CD86 and the M2 macrophage surface marker CD163. It was found that CD86 expression was lower in the Vector-ADSCs and all aFGF-ADSCs groups compared to the control group, while CD163 expression was elevated. These findings suggest that both Vector-ADSCs and aFGF-ADSCs inhibit the inflammatory response in the wound, accelerating the transition from inflammation to the cell proliferation and collagen remodeling stages. The 3×10^6 aFGF-ADSCs group showed the best anti-inflammatory effect (Fig. 5B, G, H). Sirius Red staining on day 16 was used to assess collagen remodeling. The results showed that collagen in the aFGF-ADSCs groups was denser and more orderly oriented (Fig. 5C and I). Observation under a polarized light microscope revealed a significantly higher ratio of type I collagen fibers to type III collagen fibers in the 3×10^6 aFGF-ADSCs group compared to other groups (Fig. 5D and J), indicating more mature collagen in this group's wounds.

Immunofluorescence analysis at day 16 post-treatment revealed that K10 (terminal differentiation marker) and K14 (basal layer marker) expression patterns varied among groups. The PBS group showed poor epidermal differentiation with weak expression of both K10 and K14, indicating impaired epidermal stratification. The Vector-ADSCs group demonstrated improved epidermal differentiation with slightly enhanced K10 and K14 expression. In aFGF-ADSCs groups, increased cell concentrations (from 1×10^6 to 3×10^6) resulted in progressively enhanced epidermal differentiation, as evidenced by stronger expression of both K10 and K14, suggesting better restoration of epidermal stratification. The most significant improvement was observed in the 3×10^6 aFGF-ADSCs group. However, when the concentration was further increased to 4×10^6 , these improvements showed a slight decline compared to the 3×10^6 group, suggesting that 3×10^6 might be the optimal therapeutic concentration (Fig. 5E).

aFGF-ADSCs promote wound repair by upregulating PI3K-Akt and MAPK signaling pathways

To investigate the molecular mechanisms underlying aFGF-ADSCs-mediated wound repair promotion, RNA

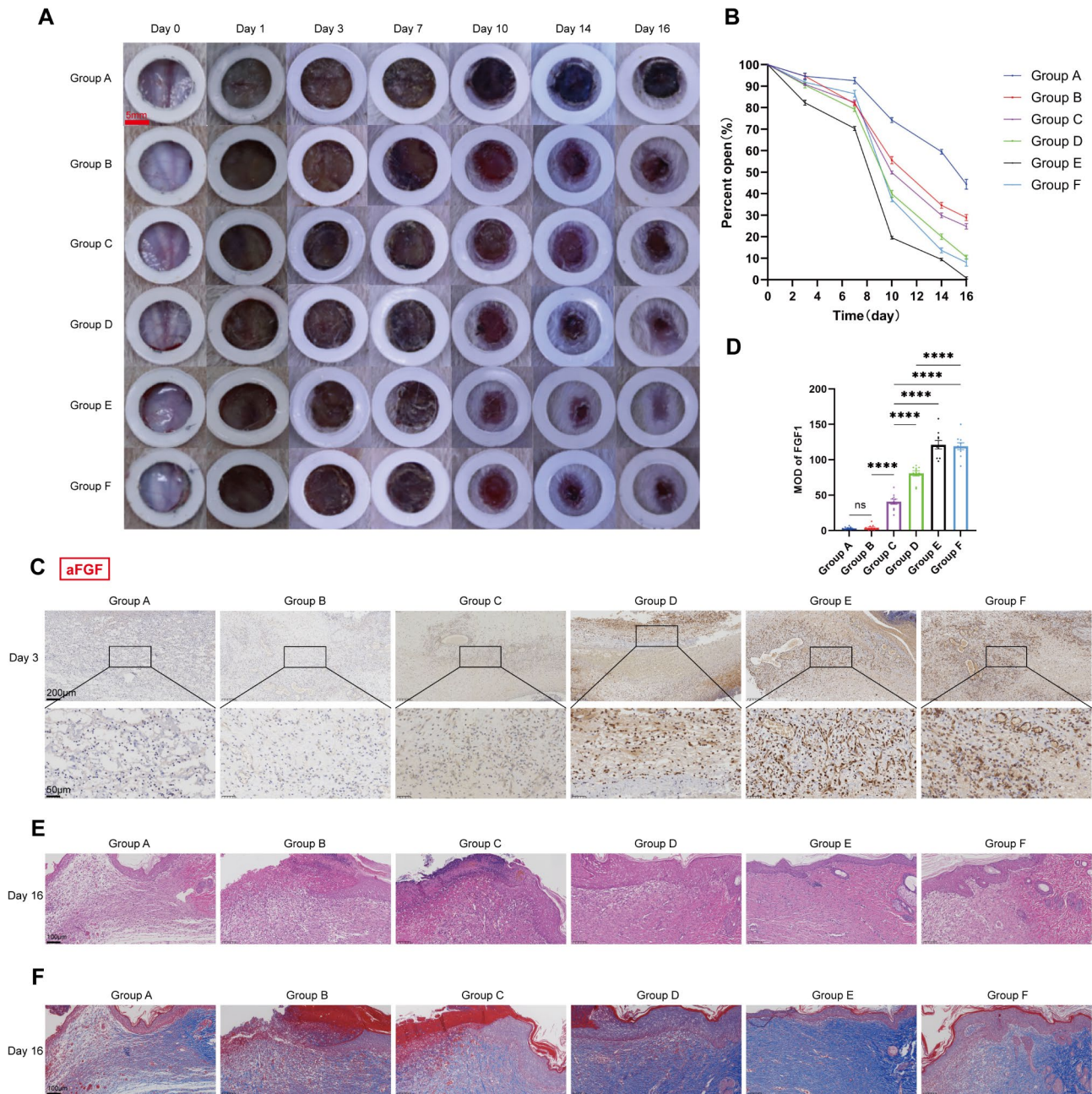


Fig. 4 Construction of a full-thickness skin defect model in diabetic rats, wound healing status, and histological analysis after treatment. Group A: PBS; Group B: 1×10^6 Vector-ADSCs; Group C: 1×10^6 aFGF-ADSCs; Group D: 2×10^6 aFGF-ADSCs; Group E: 3×10^6 aFGF-ADSCs; Group F: 4×10^6 aFGF-ADSCs. (A) Representative images of wounds in each group, showing that Vector-ADSCs and all aFGF-ADSCs groups accelerated wound healing, with Group E: 3×10^6 aFGF-ADSCs showing the best effect and complete epithelialization observed on day 16. (B) Evaluation of wound healing rates after treatment in each group. Group E: 3×10^6 aFGF-ADSCs showed significantly faster healing compared to other groups. (C) aFGF immunohistochemistry on day 3 after treatment. (D) Quantitative analysis of aFGF immunohistochemistry showed very low aFGF expression in the PBS and Vector-ADSCs groups. In the aFGF-ADSCs groups, aFGF expression in the wound tissue increased with the number of injected cells within a certain range. Group E: 3×10^6 aFGF-ADSCs and Group F: 4×10^6 aFGF-ADSCs showed the highest staining intensity, with no statistical difference between the two groups ($n = 10$). (E) Representative H&E staining images of wounds in each group on day 16 after treatment. (F) Representative Masson's trichrome staining images of wounds in each group on day 16 after treatment. ****: $p < 0.0001$; ns: $p > 0.05$

sequencing (RNAseq) was performed on P3 generation aFGF-ADSCs and Vector-ADSCs. Unsupervised principal component analysis (PCA) revealed significant differences in transcriptomic profiles between Vector-ADSCs

and aFGF-ADSCs (Fig. 6A). A total of 1664 significantly differentially expressed genes (DEGs) were identified, with 762 upregulated and 902 downregulated genes, as shown in the volcano plot (Fig. 6B).

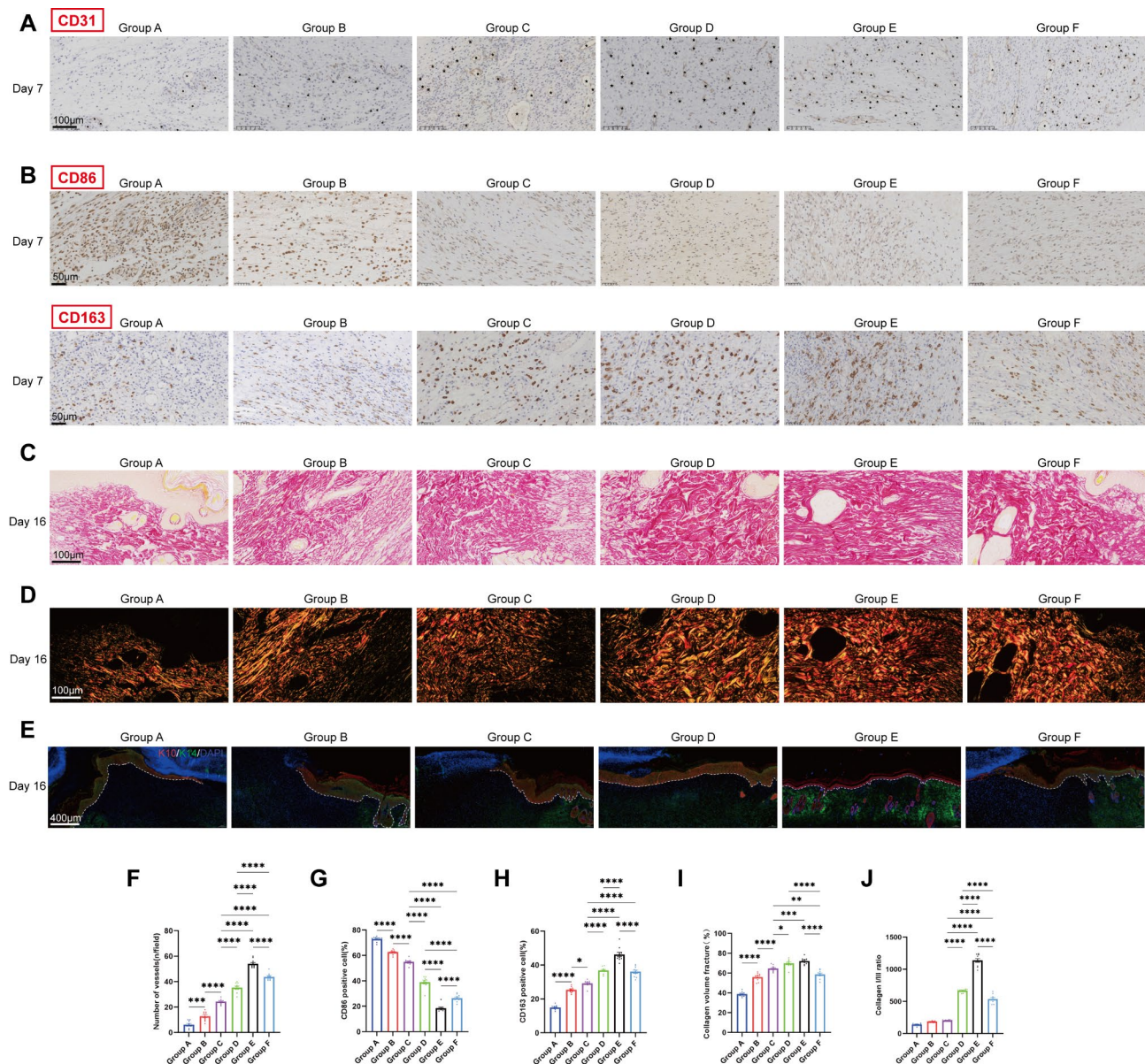


Fig. 5 Histological evaluation of full-thickness skin defect models in diabetic rats at different time points. Group **A**: PBS; Group **B**: 1×10^6 Vector-ADSCs; Group **C**: 1×10^6 aFGF-ADSCs; Group **D**: 2×10^6 aFGF-ADSCs; Group **E**: 3×10^6 aFGF-ADSCs; Group **F**: 4×10^6 aFGF-ADSCs. **(A)** Representative images of CD31 immunohistochemistry on day 7 post-treatment. **(B)** Representative images of CD86 and CD163 immunohistochemistry on day 7 post-treatment. **(C)** Representative Sirius Red staining of wound tissues from each group on day 16 post-treatment. **(D)** Representative polarized light microscopy images of wound tissues from each group on day 16 post-treatment. **(E)** Representative immunofluorescence images showing K10 (terminal differentiation marker) and K14 (basal layer marker) expression in wound tissues from each group on day 16 after treatment, demonstrating epidermal differentiation and reconstruction. **F**: Quantitative analysis of CD31-positive vessels ($n = 10$). **G**: Quantitative analysis of CD86-positive macrophages ($n = 10$). **H**: Quantitative analysis of CD163-positive macrophages ($n = 10$). **I**: Quantitative analysis of collagen in wound tissues based on Sirius Red staining **(C)** for each group ($n = 10$). **J**: Quantitative analysis of the ratio of type I collagen fibers (orange-yellow) to type III collagen fibers (green) based on polarized light microscopy of polarized light microscopy images **(D)** for each group ($n = 10$). *: $p < 0.05$; **: $p < 0.01$; ***: $p < 0.001$; ****: $p < 0.0001$; ns: $p > 0.05$

Subsequently, DEG-based enrichment analysis was performed on the up- and down-regulated gene sets. Cluster analysis clearly separated and screened the gene expression differences between Vector-ADSCs and aFGF-ADSCs (Fig. 6C). It was observed that aFGF-ADSCs, compared to the control group, showed upregulation of

genes related to angiogenesis (Angpt1, Fgf1, Fgf10, Flt1, Flt4, Hgf) and extracellular matrix remodeling (Col4a1, Col4a2, Bmp2, Mmp9, Mmp3, Lama3), while genes associated with inflammation (Ccl3, Ccl6, Ccl4, Ccl12, Fcgr2a1, Fcgr2a) were significantly downregulated (Fig. 6D).

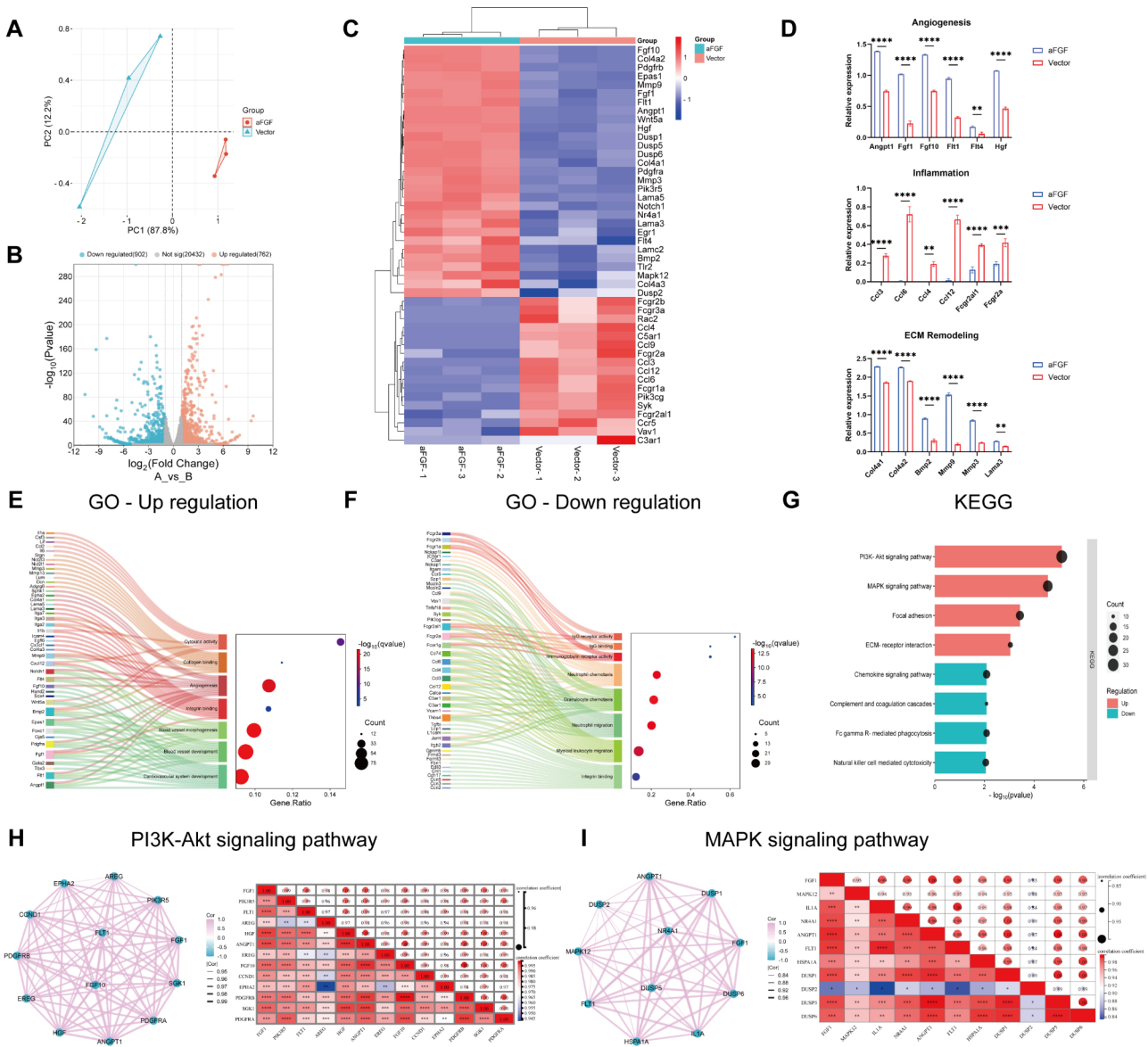


Fig. 6 RNA-seq analysis of potential molecular mechanisms by which aFGF-ADSCs promote wound healing. **(A)** Principal Component Analysis (PCA) based on differentially expressed genes (DEGs) between Vector-ADSCs and aFGF-ADSCs. **(B)** Volcano plot showing up-regulated and down-regulated genes among the DEGs. **(C)** Heatmap of up-regulated and down-regulated genes among the DEGs. **(D)** Relative expression of genes associated with key wound healing processes, including angiogenesis, inflammation, and ECM remodeling ($n=3$). **(E)** Gene Ontology (GO) enrichment analysis of up-regulated genes. **(F)** Gene Ontology (GO) enrichment analysis of down-regulated genes. **(G)** KEGG pathway analysis of differentially expressed genes. **(H)** Protein-protein interaction network and correlation analysis of up-regulated genes involved in the PI3K-Akt pathway. **(I)** Protein-protein interaction network and correlation analysis of up-regulated genes involved in the MAPK pathway

Gene Ontology (GO) analysis revealed that upregulated genes were mainly concentrated in vascular and tissue morphogenesis, cytokine activity, and collagen binding (Fig. 6E), while downregulated genes were primarily focused on inhibition of inflammatory cell migration, chemotaxis, and immune protein IgG binding (Fig. 6F). Kyoto Encyclopedia of Genes and Genomes (KEGG) pathway enrichment analysis showed that aFGF-ADSCs enhanced signal transduction in the PI3K-Akt and MAPK pathways (Fig. 6G).

Finally, correlation analysis between aFGF and key molecules in the PI3K-Akt and MAPK pathways revealed strong positive correlations between aFGF and multiple key genes in these signaling pathways, with correlation coefficients mainly ranging from 0.84 to 1.00. In the PI3K-Akt pathway, FGF1 exhibited the highest correlations with genes such as PDGFRA, PDGFRB, FGF10, and ANGPT1 (Fig. 6H). Similarly, in the MAPK pathway, FGF1 showed strong correlations with NR4A1, ANGPT1, FLT1, and HSPA1A (Fig. 6I). This high degree

of correlation suggests that FGF1 may play a crucial role in these two signaling pathways, participating in the regulation of biological processes such as cell growth, proliferation, differentiation, survival, and stress response, thereby promoting wound healing.

Discussion

Normal wound healing is a continuous, orderly linear process that includes hemostasis, inflammatory response, cell proliferation and migration, epithelialization, and remodeling [2, 30, 31]. Any disruption in this process can lead to the development of chronic wounds. Common clinical conditions associated with chronic wound pathogenesis include diabetes, venous stasis and insufficiency, and pressure injuries [32]. With societal progress and development, the incidence and life expectancy of diabetic patients have increased significantly, leading to a rise in the incidence of diabetic foot, which has become a serious social burden [33]. Therefore, there is an urgent need to develop an effective and safe treatment regimen.

ADSCs have become a research hotspot in recent years, especially in the field of wound repair. ADSCs possess multi-directional differentiation potential, self-renewal ability, and immunomodulatory properties, making them highly promising for applications in regenerative medicine [34]. They can secrete various growth factors and cytokines, such as vascular endothelial growth factor (VEGF), transforming growth factor- β (TGF- β), and hepatocyte growth factor (HGF), which can promote angiogenesis, cell proliferation, and extracellular matrix remodeling [35]. Additionally, ADSCs exhibit potent anti-inflammatory effects and can secrete anti-inflammatory factors such as interleukin-10 (IL-10) and prostaglandin E2 (PGE2) to regulate inflammatory responses, thereby accelerating wound healing [36]. These characteristics underscore the important role of ADSCs in wound repair and provide new possibilities for treating chronic wounds.

aFGF also has effects on promoting various aspects of wound healing [37, 38], and clinical studies have confirmed that local application of aFGF can significantly shorten wound healing time and reduce complications [39]. However, the optimal dosage and administration method of aFGF have not been fully determined. Different types and degrees of wounds may require tailored administration regimens, which necessitate further clinical studies for optimization [40]. Furthermore, the long-term safety and potential side effects of aFGF still need further evaluation, especially in special populations such as cancer patients [41]. These factors highlight the necessity of continuing research on the application of aFGF in wound repair to fully realize its therapeutic potential.

In this experiment, we established a diabetic rat wound model. Our preliminary results showed that the wound

healing time for diabetic rats was approximately 4 weeks, while normal rats healed in about 2 weeks. We then explored the effect of local injection of aFGF-ADSCs on wound healing. The results showed that the wound healing rates in all aFGF-ADSCs groups were higher than those of the control group and the ADSCs group, and the healing speed of the aFGF-ADSCs groups increased rapidly on day 7. The healing rate of the ADSCs group was also higher than that of the control group. Among these groups, the 3×10^6 aFGF-ADSCs group achieved complete wound epidermal coverage by day 16, although skin appendages (such as hair) had not fully recovered, while other treatment groups had not completely healed. These results suggest that both ADSCs and aFGF-ADSCs can significantly promote wound healing in diabetic rats, with aFGF and ADSCs have a synergistic effect. This synergistic effect may be related to the fact that both can promote the proliferation and migration of fibroblasts and vascular endothelial cells [29].

Next, we evaluated the role of aFGF-ADSCs in various processes of wound healing by observing histological changes in wound tissue. The results showed that aFGF-ADSCs could significantly promote early wound angiogenesis, inhibit wound inflammatory response, and make the wound enter the collagen remodeling stage earlier. In late-stage wounds, the aFGF-ADSCs treatment group exhibited richer and more orderly collagen deposition, a higher proportion of type I collagen fibers, and greater epidermal maturity. These observations indicate that aFGF-ADSCs can comprehensively improve various processes of wound repair in diabetic rats, thereby effectively promoting wound healing. This comprehensive effect of aFGF-ADSCs may represent a key mechanism underlying its significant improvement in wound healing, offering a new potential therapeutic approach for treating diabetic wounds.

The levels of aFGF in various tissues and organs in vivo are very low, and Li Xiaokun's team found that exogenous aFGF has a short half-life and no accumulation effect in vivo [42]. While direct delivery of aFGF with ADSCs to the wound site or using mRNA technology to enhance local aFGF expression are feasible options, these methods have certain limitations: co-delivery of exogenous aFGF and ADSCs may require repeated administration to maintain therapeutic effects, while mRNA has a relatively short expression duration. In contrast, lentiviral vector-mediated gene modification enables ADSCs to continuously and stably express and secrete aFGF, not only overcoming the limitations of exogenous administration but also achieving long-term gene expression.

In this study, we used gene modification technology to make ADSCs overexpress aFGF and injected them into the muscle tissue around the wound. In the early stage of wound healing (day 3), aFGF could be stably expressed

and secreted, and the staining intensity exhibited an “S”-shaped response curve with the injection concentration. This response may be related to the limited blood supply and nutritional components of the tissue surrounding the wound, which could not support cell transplantation at higher concentrations. While the present study demonstrated stable expression of aFGF in transfected ADSCs on day 3, we currently lack definitive evidence regarding the precise retention of these cells within the wound tissue. Our study was unable to track or quantify the spatial distribution, survival dynamics, and functional transitions of the transfected ADSCs within the wound micro-environment. The absence of direct cell tracking prevents us from fully understanding the mechanisms underlying the therapeutic effects of aFGF-ADSCs and limits our ability to accurately assess the duration and efficacy of the cellular treatment. This methodological limitation introduces uncertainty regarding the long-term therapeutic potential of this cell-based approach.

At the histological level of aFGF-ADSCs wounds in each group, processes such as promoting early angiogenesis, inducing macrophage polarization towards the M2 phenotype, and collagen deposition all followed a bell-shaped response curve with the injection concentration, with the best effect in various processes when the cell number was 3×10^6 . This result aligns with the findings of Hagerott et al., who reported that the single-dose effective range of local aFGF application for promoting wound repair is very narrow [28].

Viral vectors represent the most prevalent delivery system in cell and gene therapy, with established applications in oncology, metabolic disorders, neurological, and ophthalmic diseases [43]. In the present study, histological examination of aFGF-ADSCs wounds across experimental groups revealed no significant adverse pathological changes. Nevertheless, we recognize the intricate nature of safety assessment for viral vector-mediated therapies, which necessitates comprehensive and long-term investigation. The potential risks associated with viral vectors primarily include genomic instability arising from random integration sites, the possibility of replication-competent virus contamination, and the potential for unintended oncogene activation or tumor suppressor gene disruption. Despite the promising preliminary findings, we maintain a cautious stance regarding clinical translation, emphasizing the critical need for extensive long-term validation. The proposed approach, involving a single administration of 3×10^6 aFGF-ADSCs, demonstrates stable therapeutic efficacy and provides a promising continuous and controlled drug delivery strategy for diabetic wound treatment. Future research will focus on comprehensive investigations, including long-term tracking of genetically modified cells, thorough evaluation of potential genomic integration risks, in-depth assessment

of potential immunogenicity responses, and extended observation periods to detect any delayed adverse reactions.

Through RNA-seq, we found that aFGF (FGF1) showed significant positive correlations with multiple key genes in the PI3K-Akt and MAPK signaling pathways, suggesting that FGF1 may play a crucial regulatory role in these two important cellular signaling pathways. In particular, the high correlation between FGF1 and genes such as PDGFRA, PDGFRB, FGF10, and ANGPT1 (correlation coefficients close to or equal to 1.00) indicates that FGF1 may work synergistically with these factors to regulate angiogenesis, cell proliferation, and differentiation processes [44]. Angiogenesis is critical for providing oxygen and nutrients to healing tissues. Secondly, the high correlation between FGF1 and components of the PI3K-Akt pathway suggests that FGF1 may promote cell survival and proliferation by activating the PI3K-Akt pathway, which is necessary for rapid wound repair [45].

At the same time, the strong correlation between FGF1 and MAPK pathway-related genes (such as NR4A1 and the DUSP family) further supports the important role of FGF1 in cell proliferation, differentiation, and stress response [46]. This is particularly important for epithelialization and granulation tissue formation during wound healing [37]. In particular, the correlation between FGF1 and DUSP family genes suggests that FGF1 may participate in fine-tuning MAPK signaling, which may help balance inflammatory responses and tissue remodeling during the wound healing process [47].

Based on existing research, a single dose of aFGF-ADSCs has demonstrated significant effects in promoting wound healing in diabetic rats. Through RNA-seq analysis, we observed a remarkable correlation between FGF1 and multiple key genes in the PI3K-Akt and MAPK signaling pathways. However, the precise mechanisms by which these signaling pathways regulate angiogenesis and macrophage function remain incompletely understood.

The PI3K-Akt signaling pathway plays a crucial role in angiogenesis [48]. Studies have revealed that this pathway promotes endothelial cell function through multiple mechanisms: by activating downstream mTOR and HIF-1 α , it upregulates VEGF expression, stimulating endothelial cell proliferation and tube formation [49]. Simultaneously, through endothelial nitric oxide synthase (eNOS) phosphorylation, it promotes nitric oxide (NO) production, enhancing vascular dilation and endothelial cell migration [49, 50].

The MAPK signaling pathway plays a crucial role in wound healing, with p38 primarily regulating early inflammatory responses by promoting pro-inflammatory cytokines such as TNF- α , IL-1 β , and IL-6, and modulating macrophage and neutrophil inflammatory responses [51]. ERK1/2, in contrast, predominantly participates in

later tissue repair processes by promoting fibroblast proliferation, collagen synthesis, and angiogenesis. Through regulation of transcription factors like STAT3 and PPAR γ , ERK1/2 guides macrophages towards an anti-inflammatory and repair phenotype, thereby maintaining the immune microenvironment of wound healing. This fine-tuned regulation of different MAPK pathway branches collectively drives the complex transformation of wounds from inflammation to repair [52, 53].

Nevertheless, the mechanisms by which aFGF regulates these signaling pathways in ADSCs require further exploration in future research to comprehensively elucidate the therapeutic mechanisms of aFGF-ADSCs in wound healing.

Conclusion

In summary, this study confirms that a single dose of aFGF-ADSCs has a significant promoting effect on wound healing in diabetic rats, showing a clear dose-dependency. The potential mechanism involves improving multiple key aspects of wound repair, including promoting neovascularization, inhibiting inflammatory responses, accelerating wound epithelialization, and optimizing collagen deposition. These comprehensive effects collectively contribute to an overall improvement in the wound healing process. This research provides a novel and promising treatment option for diabetic chronic wounds, laying an important experimental foundation for future clinical applications. Although further studies are needed to verify its long-term safety and effectiveness in humans, the aFGF-ADSCs treatment strategy demonstrates potential to become a valuable addition to the management of diabetic chronic wounds.

Abbreviations

ADSCs	Adipose-derived mesenchymal stem cells
aFGF/FGF1	Acidic fibroblast growth factor
ECM	Extracellular matrix
VEGF	Vascular endothelial growth factor
HGF	Hepatocyte growth factor
bFGF	Basic fibroblast growth factor
α -SMA	α -smooth muscle actin
VECs	Vascular endothelial cells
SD	Sprague-Dawley
PBS	Phosphate-buffered saline
H&E	Hematoxylin-eosin staining
MSC	Mesenchymal stem cell
RNAseq	RNA sequencing
PCA	Principal component analysis
DEGs	Differentially expressed genes
GO	Gene Ontology
KEGG	Kyoto Encyclopedia of Genes and Genomes
TGF- β	Transforming growth factor- β
IL-10	Interleukin-10
PGE2	Prostaglandin E2
CO $_2$	Subscript>2</Subscript> Carbon Dioxide
IACUC	Institutional Animal Care and Use Committee

Supplementary Information

The online version contains supplementary material available at <https://doi.org/10.1186/s13287-025-04241-5>.

Supplementary Material 1

Acknowledgements

We thank Shanghai GeneChem Co., Ltd for providing plasmid synthesis services, Shanghai Sangon Biotech for providing primer synthesis services, Sunya Biotechnology Co., Ltd for providing plasmid sequencing services, Beijing Berry Genomics Corporation for providing RNA-seq services, and Mingjie Chen (Shanghai NewCore Biotechnology Co., Ltd.) for providing data analysis and visualization support. The authors declare that artificial intelligence is not used in this study.

Author contributions

H. conceived and designed the experiments. Y.Z., Q.F., P.Ch., R.W., and X.H. performed the experiments. Y.Z., Z.Z., P.Ch., and X.H. analyzed the data. Y.Z., Z.Z., P.Ch., and X.H. wrote the paper. All authors reviewed the manuscript.

Funding

This study was supported by Natural Science Foundation of Fujian Province (Fujian Provincial Natural Science Foundation): (Grant number:2024J011027); Science and Technology Innovation Joint Fund Project of Fujian Province: (Grant number: 2023Y9323); Fujian Medical Innovation Project: (Grant number: 2020CXA007).

Data availability

RNAseq data is available in the Sequence Read Archive (SRA) under code PRJNA1194048 (<https://www.ncbi.nlm.nih.gov/sra/?term=PRJNA1194048>). Additional data requests should be directed to the corresponding author.

Declarations

Ethics approval and consent to participate

All animal experiments were rigorously reviewed and approved by the Institutional Animal Care and Use Committee (IACUC) of Fujian Provincial Hospital, Fujian, China. The research encompassed two distinct projects: the first investigating the "Biological Effects and Mechanisms of aFGF Gene-modified Adipose-Derived Stem Cells (ADSCs) in the Treatment of Refractory Diabetic Wounds" (approval number IACUC-FPH-SL-20240321, granted on March 21, 2024), and the second exploring the "Role and Mechanism of Pak2 Protein in MAPK Signaling Pathway during BMP-2 and TGF- β Synergistic Promotion of Osteogenic Differentiation in Bone Marrow Stromal Cells" (approval number IACUC-FPH-SL-20240403[0232], granted on April 3, 2024). The Fujian Academy of Medical Sciences held a valid Experimental Animal Use License (SYXK 2016-0004) during the conduct of these studies.

Consent for publication

All co-authors have seen and agree with the contents of the manuscript for publication.

Disclosures

No conflicts of interest, financial or otherwise, are declared by the authors.

Received: 4 December 2024 / Accepted: 17 February 2025

Published online: 25 February 2025

References

1. Kanitakis J. Anatomy, histology and immunohistochemistry of normal human skin. *Eur J Dermatol*. 2002;12(4):390-9. PMID: 12095893.
2. Eming SA, Martin P, Tomic-Canic M. Wound repair and regeneration: mechanisms, signaling, and translation. *Sci Transl Med*. 2014;6(265):265sr6. <https://doi.org/10.1126/scitranslmed.3009337>. PMID: 25473038; PMCID: PMC4973620.
3. Xue M, Zhao R, Lin H, Jackson C. Delivery systems of current biologicals for the treatment of chronic cutaneous wounds and severe burns. *Adv Drug*

- Deliv Rev. 2018;129:219–41. <https://doi.org/10.1016/j.addr.2018.03.002>. Epub 2018 Mar 19. PMID: 29567398.
4. Frykberg RG, Banks J. Challenges in the Treatment of Chronic Wounds. *Adv Wound Care* (New Rochelle). 2015;4(9):560–82. <https://doi.org/10.1089/wound.2015.0635>. PMID: 26339534; PMCID: PMC4528992.
 5. Kim JH, Yang B, Tedesco A, Lebig EGD, Ruegger PM, Xu K, Borneman J, Martins-Green M. High levels of oxidative stress and skin Microbiome are critical for initiation and development of chronic wounds in diabetic mice. *Sci Rep*. 2019;9(1):19318. <https://doi.org/10.1038/s41598-019-55644-3>. PMID: 31848388; PMCID: PMC6917777.
 6. Huang YZ, Gou M, Da LC, Zhang WQ, Xie HQ. Mesenchymal stem cells for chronic wound healing: current status of preclinical and clinical studies. *Tissue Eng Part B Rev*. 2020;26(6):555–70. <https://doi.org/10.1089/ten.TEB.2019.0351>. Epub 2020 May 20. PMID: 32242479.
 7. Nussbaum SR, Carter MJ, Fife CE, DaVanzo J, Haught R, Nussbaum M, Cartwright D. An economic evaluation of the impact, cost, and medicare policy implications of chronic nonhealing wounds. *Value Health*. 2018;21(1):27–32. Epub 2017 Sep 19. PMID: 29304937.
 8. Kaviani M, Geramizadeh B. Basic aspects of skin tissue engineering: cells, biomaterials, scaffold fabrication techniques, and signaling factors. *J Med Biol Eng*. 2023;43(4):508–21. <https://doi.org/10.1007/s40846-023-00822-y>.
 9. Bi H, Jin Y. Current progress of skin tissue engineering: seed cells, bioscaffolds, and construction strategies. *Burns Trauma*. 2013;1(2):63–72. <https://doi.org/10.4103/2321-3868.118928>. PMID: 27574627; PMCID: PMC4978104.
 10. Chan BP, Leong KW. Scaffolding in tissue engineering: General approaches and tissue-specific considerations. *Eur Spine J*. 2008;17(Suppl 4):467–79. <https://doi.org/10.1007/s00586-008-0745-3>. Epub 2008 Nov 13. PMID: 19005702; PMCID: PMC2587658.
 11. Singh D, Singh D, Han SS. 3D printing of scaffold for cells delivery: advances in skin tissue engineering. *Polym (Basel)*. 2016;8(1):19. <https://doi.org/10.3390/polym8010019>. PMID: 30979115; PMCID: PMC6432526.
 12. Shimojo AAM, Rodrigues ICP, Perez AGM, Souto EMB, Gabriel LP, Webster T. Scaffolds for tissue engineering: A state-of-the-art review concerning types, properties, materials, processing, and characterization. In: Li B, Moriarty T, Webster T, Xing M, editors. *Racing for the surface*. Springer; 2020. pp. 1–15. https://doi.org/10.1007/978-3-030-34471-9_23.
 13. Bacakova L, Zarubova J, Travnickova M, Musilkova J, Pajorova J, Slepicka P, Kasalkova NS, Svorcik V, Kolska Z, Motarjemi H, Molitor M. Stem cells: Their source, potency, and use in regenerative therapies with focus on adipose-derived stem cells—A review. *Biotechnol Adv*. 2018;36(4):1111–26. <https://doi.org/10.1016/j.biotechadv.2018.03.011>. Epub 2018 Mar 18. PMID: 29563048.
 14. Tobita M, Orbay H, Mizuno H. Adipose-derived stem cells: current findings and future perspectives. *Discov Med*. 2011;11(57):160–70. PMID: 21356171.
 15. Nishiwaki K, Aoki S, Kinoshita M, Kiyosawa T, Suematsu Y, Takeoka S, Fujie T. In situ transplantation of adipose tissue-derived stem cells organized on porous polymer nanosheets for murine skin defects. *J Biomed Mater Res B Appl Biomater*. 2019;107(5):1363–71. <https://doi.org/10.1002/jbm.b.34228>. Epub 2018 Sep 28. PMID: 30265776.
 16. Li P, Guo X. A review: therapeutic potential of adipose-derived stem cells in cutaneous wound healing and regeneration. *Stem Cell Res Ther*. 2018;9(1):302. <https://doi.org/10.1186/s13287-018-1044-5>. PMID: 30409218; PMCID: PMC6225584.
 17. Li Y, Zhang W, Gao J, Liu J, Wang H, Li J, Yang X, He T, Guan H, Zheng Z, Han S, Dong M, Han J, Shi J, Hu D. Adipose tissue-derived stem cells suppress hypertrophic Scar fibrosis via the p38/MAPK signaling pathway. *Stem Cell Res Ther*. 2016;7(1):102. <https://doi.org/10.1186/s13287-016-0356-6>. PMID: 27484727; PMCID: PMC4970202.
 18. Hancar G, Liu S, Gasser E, Alvarez JG, Moutos C, Kim K, van Zutphen T, Wang Y, Hundty TF, Ross B, Dai Y, Zepeda D, Collins B, Tilley E, Kolar MJ, Yu RT, Atkins AR, van Dijk TH, Saghatelian A, Jonker JW, Downes M, Evans RM. FGF1 and insulin control lipolysis by convergent pathways. *Cell Metab*. 2022;34(1):171–83. <https://doi.org/10.1016/j.cmet.2021.12.004>. PMID: 34986332; PMCID: PMC8863067.
 19. Scarlett JM, Rojas JM, Matsen ME, Kaiyala KJ, Stefanovski D, Bergman RN, Nguyen HT, Dorfman MD, Lantier L, Wasserman DH, Mirzadeh Z, Unterman TG, Morton GJ, Schwartz MW. Central injection of fibroblast growth factor 1 induces sustained remission of diabetic hyperglycemia in rodents. *Nat Med*. 2016;22(7):800–6. <https://doi.org/10.1038/nm.4101>. Epub 2016 May 23. PMID: 27213816; PMCID: PMC4938755.
 20. Suh JM, Jonker JW, Ahmadian M, Goetz R, Lackey D, Osborn O, Huang Z, Liu W, Yoshihara E, van Dijk TH, Havinga R, Fan W, Yin YQ, Yu RT, Liddle C, Atkins AR, Olefsky JM, Mohammadi M, Downes M, Evans RM. Endocrinization of FGF1 produces a neomorphic and potent insulin sensitizer. *Nature*. 2014;513(7518):436–9. <https://doi.org/10.1038/nature13540>. Epub 2014 Jul 16. Erratum in: *Nature*. 2015;520(7547):388. doi: 10.1038/nature14304. PMID: 25043058; PMCID: PMC4184286.
 21. Maciag T, Cerundolo J, Ilsley S, Kelley PR, Forand R. An endothelial cell growth factor from bovine hypothalamus: identification and partial characterization. *Proc Natl Acad Sci U S A*. 1979;76(11):5674–8. <https://doi.org/10.1073/pnas.76.11.5674>. PMID: 293671; PMCID: PMC411712.
 22. Thornton SC, Mueller SN, Levine EM. Human endothelial cells: use of heparin in cloning and long-term serial cultivation. *Science*. 1983;222(4624):623–5. <https://doi.org/10.1126/science.6635659>. PMID: 6635659.
 23. Maciag T, Mehlman T, Friesel R, Schreiber AB. Heparin binds endothelial cell growth factor, the principal endothelial cell mitogen in bovine brain. *Science*. 1984;225(4665):932–5. <https://doi.org/10.1126/science.6382607>. PMID: 6382607.
 24. Shipley GD, Keeble WW, Hendrickson JE, Coffey RJ Jr, Pittelkow MR. Growth of normal human keratinocytes and fibroblasts in serum-free medium is stimulated by acidic and basic fibroblast growth factor. *J Cell Physiol*. 1989;138(3):511–8. <https://doi.org/10.1002/jcp.1041380310>. PMID: 2466852.
 25. Thomas KA, Rios-Candelore M, Giménez-Gallego G, DiSalvo J, Bennett C, Rodkey J, Fitzpatrick S. Pure brain-derived acidic fibroblast growth factor is a potent angiogenic vascular endothelial cell mitogen with sequence homology to Interleukin 1. *Proc Natl Acad Sci U S A*. 1985;82(19):6409–13. <https://doi.org/10.1073/pnas.82.19.6409>. PMID: 2413439; PMCID: PMC390725.
 26. Linemeyer D, Kelly L, Menke J, et al. Expression in *Escherichia coli* of a chemically synthesized gene for biologically active bovine acidic fibroblast growth factor. *Nat Biotechnol*. 1987;5(10):960–5. <https://doi.org/10.1038/nbt0987-960>.
 27. Blaber SI, Diaz J, Blaber M. Accelerated healing in NONcNZO10/LtJ type 2 diabetic mice by FGF-1. *Wound Repair Regen*. 2015;23(4):538–49. <https://doi.org/10.1111/wrr.12305>. PMID: 25891187.
 28. Hagerott BN, Blumstein AJ, McGarry LE, et al. A bell-shaped dose-response of topical FGF-1 in accelerating dermal wound healing in aged female BALB/cByJ mice. *J Proteins Proteom*. 2020;11:183–91. <https://doi.org/10.1007/s4248-020-00040-z>.
 29. Hoseini SJ, Ghazavi H, Forouzanfar F, Mashkani B, Ghorbani A, Mahdipour E, Ghasemi F, Sadeghnia HR, Ghayour-Mobarhan M. Fibroblast growth factor 1-transfected adipose-derived mesenchymal stem cells promote angiogenic proliferation. *DNA Cell Biol*. 2017;36(5):401–12. <https://doi.org/10.1089/dna.2016.3546>. Epub 2017 Mar 10. PMID: 28281780; PMCID: PMC5421621.
 30. Rodrigues M, Kosaric N, Bonham CA, Gurtner GC. Wound healing: A cellular perspective. *Physiol Rev*. 2019;99(1):665–706. <https://doi.org/10.1152/physrev.00067.2017>. PMID: 30475656; PMCID: PMC6442927.
 31. Falanga V. Wound healing and its impairment in the diabetic foot. *Lancet*. 2005;366(9498):1736–43. [https://doi.org/10.1016/S0140-6736\(05\)67700-8](https://doi.org/10.1016/S0140-6736(05)67700-8). PMID: 16291068.
 32. Sen CK. Human wound and its burden: Updated 2020 compendium of estimates. *Adv Wound Care* (New Rochelle). 2021;10(5):281–92. <https://doi.org/10.1089/wound.2021.0026>. PMID: 33733885; PMCID: PMC8024242.
 33. Zhang P, Lu J, Jing Y, Tang S, Zhu D, Bi Y. Global epidemiology of diabetic foot ulceration: a systematic review and meta-analysis. *Ann Med*. 2017;49(2):106–16. <https://doi.org/10.1080/07853890.2016.1231932>. Epub 2016 Nov 3. PMID: 27585063.
 34. Mazini L, Rochette L, Admou B, Amal S, Malka G. Hopes and limits of adipose-derived stem cells (ADSCs) and mesenchymal stem cells (MSCs) in wound healing. *Int J Mol Sci*. 2020;21(4):1306. <https://doi.org/10.3390/ijms21041306>. PMID: 32075181; PMCID: PMC7072889.
 35. Hassanshahi A, Hassanshahi M, Khabbazi S, Hosseini-Khah Z, Peymanfar Y, Ghalamkari S, Su YW, Xian CJ. Adipose-derived stem cells for wound healing. *J Cell Physiol*. 2019;234(6):7903–14. <https://doi.org/10.1002/jcp.27922>. Epub 2018 Dec 4. PMID: 30515810.
 36. Suga H, Eto H, Aoi N, Kato H, Araki J, Doi K, Higashino T, Yoshimura K. Adipose tissue remodeling under ischemia: death of adipocytes and activation of stem/progenitor cells. *Plast Reconstr Surg*. 2010;126(6):1911–23. <https://doi.org/10.1097/PRS.0b013e3181f4468b>. PMID: 21124131.
 37. Yun YR, Won JE, Jeon E, Lee S, Kang W, Jo H, Jang JH, Shin US, Kim HW. Fibroblast growth factors: biology, function, and application for tissue regeneration. *J Tissue Eng*. 2010;2010:218142. <https://doi.org/10.4061/2010/218142>. PMID: 21350642; PMCID: PMC3042641.
 38. Nunes QM, Li Y, Sun C, Kinnunen TK, Fernig DG. Fibroblast growth factors as tissue repair and regeneration therapeutics. *PeerJ*. 2016;4:e1535. <https://doi.org/10.7717/peerj.1535>. PMID: 26793421; PMCID: PMC4715458.

39. Ma B, Cheng DS, Xia ZF, Ben DF, Lu W, Cao ZF, Wang Q, He J, Chai JK, Shen CA, Sun YH, Zhang GA, Hu XH. Randomized, multicenter, double-blind, and placebo-controlled trial using topical recombinant human acidic fibroblast growth factor for deep partial-thickness burns and skin graft donor site. *Wound Repair Regen*. 2007;15(6):795–9. <https://doi.org/10.1111/j.1524-475X.2007.00307.x>. PMID: 18028126.
40. Akita S, Akino K, Imaizumi T, Hirano A. Basic fibroblast growth factor accelerates and improves second-degree burn wound healing. *Wound Repair Regen*. 2008;16(5):635–41. <https://doi.org/10.1111/j.1524-475X.2008.00414.x>. PMID: 19128258.
41. Beenken A, Mohammadi M. The FGF family: biology, pathophysiology and therapy. *Nat Rev Drug Discov*. 2009;8(3):235–53. <https://doi.org/10.1038/nrd2792>. PMID: 19247306; PMCID: PMC3684054.
42. Huang Z, Lu M, Zhu G, Gao H, Xie L, Zhang X, Ye C, Wang Y, Sun C, Li X. Acceleration of diabetic-wound healing with PEGylated rhaFGF in healing-impaired streptozocin diabetic rats. *Wound Repair Regen*. 2011;19(5):633–44. <https://doi.org/10.1111/j.1524-475X.2011.00722.x>. PMID: 22092801.
43. Lundstrom K. Viral vectors in gene therapy: where do we stand in 2023? *Viruses*. 2023;15(3):698. <https://doi.org/10.3390/v15030698>. PMID: 36992407; PMCID: PMC10059137.
44. Ornitz DM, Itoh N. The fibroblast growth factor signaling pathway. *Wiley Interdiscip Rev Dev Biol*. 2015;4(3):215–66. <https://doi.org/10.1002/wdev.176>. Epub 2015 Mar 13. PMID: 25772309; PMCID: PMC4393358.
45. Karar J, Maity A. PI3K/AKT/mTOR pathway in angiogenesis. *Front Mol Neurosci*. 2011;4:51. <https://doi.org/10.3389/fnmol.2011.00051>. PMID: 22144946; PMCID: PMC3228996.
46. Mossahebi-Mohammadi M, Quan M, Zhang JS, Li X. FGF signaling pathway: a key regulator of stem cell pluripotency. *Front Cell Dev Biol*. 2020;8:79. <https://doi.org/10.3389/fcell.2020.00079>. PMID: 32133359; PMCID: PMC7040165.
47. Portou MJ, Baker D, Abraham D, Tsui J. The innate immune system, toll-like receptors and dermal wound healing: a review. *Vascul Pharmacol*. 2015;71:31–6. <https://doi.org/10.1016/j.vph.2015.02.007>. Epub 2015 Apr 11. PMID: 25869514.
48. Han X, Zhang G, Chen G, Wu Y, Xu T, Xu H, Liu B, Zhou Y. Buyang Huanwu Decoction promotes angiogenesis in myocardial infarction through suppression of PTEN and activation of the PI3K/Akt signalling pathway. *J Ethnopharmacol*. 2022;287:114929. <https://doi.org/10.1016/j.jep.2021.114929>. PMID: 34952189.
49. Shen K, Ji L, Gong C, Ma Y, Yang L, Fan Y, Hou M, Wang Z. Notoginsenoside Ft1 promotes angiogenesis via HIF-1 α mediated VEGF secretion and the regulation of PI3K/AKT and Raf/MEK/ERK signaling pathways. *Biochem Pharmacol*. 2012;84(6):784–92. <https://doi.org/10.1016/j.bcp.2012.05.024>. PMID: 22771629.
50. Chung BH, Kim JD, Kim CK, Kim JH, Won MH, Lee HS, Dong MS, Ha KS, Kwon YG, Kim YM. Icaritin stimulates angiogenesis by activating the MEK/ERK- and PI3K/Akt/eNOS-dependent signal pathways in human endothelial cells. *Biochem Biophys Res Commun*. 2008;376(2):404–8. <https://doi.org/10.1016/j.bbrc.2008.09.001>. PMID: 18789310.
51. Li D, Pan L, Zhang X, Jiang Z. Lower oligomeric form of surfactant protein D in murine acute lung injury induces M1 subtype macrophages through Calreticulin/p38 MAPK signaling pathway. *Front Immunol*. 2021;12:687506. <https://doi.org/10.3389/fimmu.2021.687506>. PMID: 34484184; PMCID: PMC8415422.
52. Son ES, Park JW, Kim SH, Park HR, Han W, Kwon OC, Nam JY, Jeong SH, Lee CS. Anti-inflammatory activity of 3,5,6,7,3',4'-hexamethoxyflavone via repression of the NF- κ B and MAPK signaling pathways in LPS-stimulated RAW264.7 cells. *Mol Med Rep*. 2020;22(3):1985–93. <https://doi.org/10.3892/mmr.2020.11252>. PMID: 32705181; PMCID: PMC7411374.
53. Zhang SM, Wei CY, Wang Q, Wang L, Lu L, Qi FZ. M2-polarized macrophages mediate wound healing by regulating connective tissue growth factor via AKT, ERK1/2, and STAT3 signaling pathways. *Mol Biol Rep*. 2021;48(9):6443–6456. <https://doi.org/10.1007/s11033-021-06646-w>. PMID: 34398425.

Publisher's note

Springer Nature remains neutral with regard to jurisdictional claims in published maps and institutional affiliations.